Deflection of the Interstellar Neutral Hydrogen Flow Across the Heliospheric Interface

R. Lallement,[1]* E. Quémerais,[1] J. L. Bertaux,[1] S. Ferron,[1] D. Koutroumpa,[1] R. Pellinen[2]

Using an absorption cell, we measured the Doppler shifts of the interstellar hydrogen resonance glow to show the direction of the neutral hydrogen flow as it enters the inner heliosphere. The neutral hydrogen flow is found to be deflected relative to the helium flow by about 4°. The most likely explanation of this deflection is a distortion of the heliosphere under the action of an ambient interstellar magnetic field. In this case, the helium flow vector and the hydrogen flow vector constrain the direction of the magnetic field and act as an interstellar magnetic compass.

The Sun is moving at a velocity of 25.5 km s^{-1} through a tenuous, 20 to 30% ionized interstellar cloud (1–3). The inflowing interstellar plasma forces the solar wind to turn back and confines it within the heliosphere, whereas the interstellar plasma is diverted around the heliopause (4). Interstellar neutral species separate from the plasma, cross the heliospheric interface, and reach the inner solar system, forming the so-called interstellar wind (5). However, this separation is not complete because of charge-transfer reactions between ions and atoms, which, beyond the heliopause, have a characteristic length scale on the order of the size of the heliosphere [≈100 astronomical units (AU)]. This process replaces a fraction of the initial interstellar H atoms with a new population of atoms that are instantaneously moving in the same direction and at the same speed as the decelerated and heated interstellar protons (6–8). Unlike H, neutral He experiences much less charge transfer and, when entering the heliosphere, keeps the characteristics of the ambient circumsolar interstellar medium (2). The differences between the neutral H flow and that of neutral He (i.e., the deceleration, heating, and filtering of neutral H), because they measure the imprints of the plasma, constrain the plasma flow properties and the heliospheric interface structure and size (9–13).

The direction and strength of the interstellar magnetic field B_{IS} in the solar neighborhood are unknown. Measurements over large distances show that galactic magnetic field intensities are on the order of a few microgauss. Therefore, the ambient interstellar magnetic pressure may be large compared with the gas pressure and thus may influence the size and shape of the heliosphere. There is no physical reason for any particular angle between the heliocentric-wind vector (which depends on the random motion of the Sun) and the magnetic field vector (which depends on the history of the local interstellar medium and the interaction of the local cloud with other clouds). As a consequence, an additional magnetic confinement of the heliosphere is likely to produce departures from axial symmetry of the heliospheric plasma interface, and, in turn, the detection of a difference between the H and He flow directions would be a sign for such an asymmetry of the plasma distribution.

The solar wind anisotropies (SWAN) experiment (14) on board the Solar and Heliospheric Observatory (SOHO) satellite is mapping the solar Lyman-α (Ly-α) radiation (with a wavelength of 121.6 nm) that is resonantly backscattered by interstellar H atoms, called the H glow. Most of the glow is generated within ≈10 AU from the Sun. When activated, an absorption cell blocks out a fraction of the emission line [supporting online material (SOM) text 1]. The absorption line's Doppler shift depends on the relative motion between the emitter (the interstellar H flow) and the absorber (the cell or the spacecraft). To first order, the transmitted fraction is a minimum for a line of sight that is perpendicular to the relative-velocity vector. The locations on the sky of the maximum absorption directions form a pattern that is close to a circle, called the zero–Doppler shift circle (ZDSC) (SOM text 2). During the year, the gas velocity in the SOHO frame changes in modulus and direction, and the ZDSC changes accordingly (Fig. 1). A cell thus acts as a negative scanning spectrometer, providing information on the emission line and thus the velocity distribution of the interstellar atoms.

We extracted several series of data points forming secants of the ZDSC (Fig. 1). Within each series, the direction of sight moves from one side to the other of the ZDSC. Along each of these secants, we derived the coordinates of the minimum transmission

[1]Service d'Aéronomie du Centre National de la Recherche Scientifique, Institut Pierre Simon Laplace, Boite Postale 3, 91371 Verrières-le-Buisson, France. [2]Finnish Meteorological Institute, Post Office Box 503, 00101 Helsinki, Finland.

*To whom correspondence should be addressed. E-mail: rosine.lallement@aerov.jussieu.fr

Fig. 1. Two examples of absorption cell transmission maps recorded by SOHO/SWAN (on 25 April 1996 and 29 December 1996). Maps are in ecliptic coordinates. Blank areas correspond to the absence of measurements or to contaminated data. Maximum absorption directions (green areas) form a pattern close to a great circle. This ZDSC is in a plane that is perpendicular to the interstellar gas velocity in the observer frame, i.e., the difference between the H flow motion (green dashed vector) and the Earth velocity (black vector). The data used for the present analysis (black dots) are series of secants of the ZDSC.
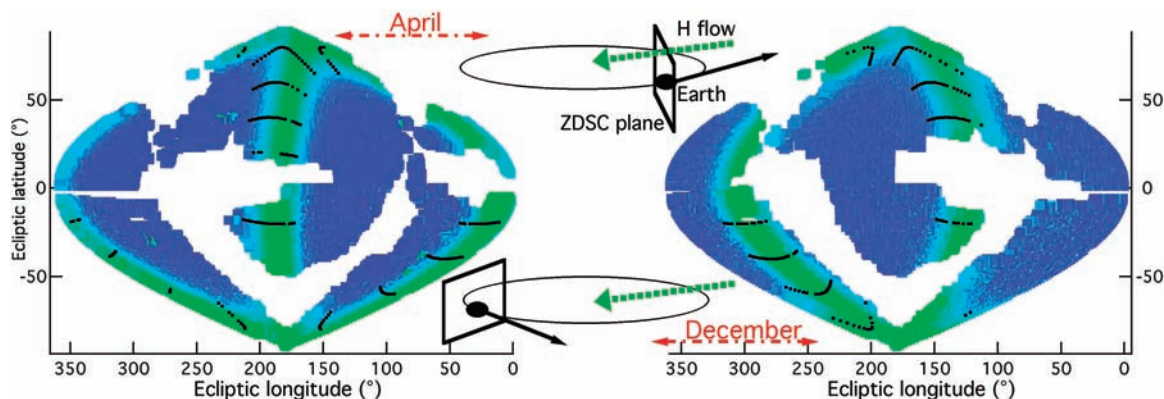
direction (SOM text 3). In parallel, we calculated the transmission predicted by a forward model of a homogeneous, single-fluid, neutral H flow (SOM text 4) and derived the coordinates of the predicted minimum-transmission direction. Finally, for each secant, we calculated the angle between the measured and modeled directions. The model has been adjusted to the data by minimizing these angles using a least squares method.

Our method uses the line Doppler shifts only, which allows us to neglect the cell characteristics and their temporal variations (aging), as well as line broadening caused by radiative transfer of photons (SOM text 5) (15). We performed a parametric study within the optically thin assumption (photons are scattered once), and we varied, in addition to the wind's direction, its bulk velocity and its temperature. The ratio of radiation pressure to solar gravity was also varied between 0.8 and 1.0 (11, 16). We used the self-reversed solar line measured as in (17). The rate of ionization under the influence of the solar wind and solar extreme-ultraviolet photons was varied between 1.0×10^{-6} and 1.5×10^{-6} s^{-1} at 1 AU, and a 40% decrease of the ionization between the Sun's equator and the pole was assumed. The derived bulk speed (22 ± 1.0 km s^{-1}) and the derived temperature of the incoming H flow (11,500 ± 1000 K) (SOM text 6) are similar to previous measurements (10, 11). These derived measurements, when compared with He measurements (bulk speed of 26.3 ± 0.4 km s^{-1} and temperature of 6300 ± 340K) from (18, 19), confirm the deceleration and heating of the H flow. The minimum reduced

χ^2 is found for (λ, β) = (252.5°, 8.8°, where λ is the ecliptic longitude and β is the ecliptic latitude).

A different, model-independent method of line profile reconstruction (12) was also applied to the same data. By combining measurements taken toward the same given direction in the sky and recorded from all the SOHO vantage points during a year (i.e., with varying Doppler shifts of the cell absorption line), it is possible to fully or partially reconstruct the line profile corresponding to this given direction. By using the resulting map of projected velocities, we found the wind axis (12) to vary in a systematic way from the upwind to the downwind side [from (λ, β) ≈ (249°, 8°) to (λ, β) ≈ (253°, 9.5°)], as if the flow were rotating by about 3° to 4° around the Sun. This trend has raised some doubts about the possibility of comparing the direction of H flow with the direction of He flow. We used our model to perform a test of this method and found that this shift is mainly caused by the assumption that the line profile from a given direction is independent of the location of the observer along Earth's orbit (SOM text 7) (12). We used this analysis to calculate corrections to the earlier results of (12). After correction, the wind directions are less scattered and are centered on (λ, β) = (252.2°, 9.0°) (Fig. 2). The two independent methods, a data-model adjustment of the ZDSC location and the model-independent line profile reconstruction, are consistent (SOM text 8). We have considered the difference between the two results as representative of the uncertainties on the wind axis direction; that is, our error bars are on the order of 0.5° and take into account the existence of residual systematic effects caused by our monofluid approxi-

mation, departures from stationariness, or solar wind anisotropies (SOM text 8).

Interstellar neutral He has been found to flow from (λ, β) = (254.7° ± 0.4°, 5.2° ± 0.2°) (18–20), which is different from the H flow direction by 4° ± 1°. The reason for such a deviation of the H flow is most likely linked to a distortion of the heliosphere, probably under the action of an ambient B_{IS}. Other explanations are less likely, but the most serious other candidate is a combination of strong solar wind latitudinal anisotropies and a strong north-south solar wind asymmetry (SOM text 9). A number of magneto-hydrodynamic (MHD) models of the heliosphere in the case of an inclined interstellar magnetic field that include a simplified treatment of charge exchange have been calculated (21–23), but no fully self-consistent model has been built yet.

A common feature of the models, including pure MHD models (24), is a large distortion of the bow shock and the heliopause (Fig. 3) for 30° < α < 60°, where α is the angle between B_{IS} and the bulk-flow velocity vector V (both the field-aligned flow and the perpendicular case lead to axisymmetry). A fraction of the H atoms that reach the Sun come directly from the interstellar medium. This is the so-called primary component (flow 1 in Fig. 3), which keeps its initial direction (the He flow direction). A second flow of neutral atoms reaching the inner solar system is made of the transcharged (neutralized by charge transfer) interstellar protons, the so-called secondary atoms (flow 2). Most of those secondaries are born in the outer heliosheath between the bow shock and the heliopause (8). The major difference between the secondaries in the
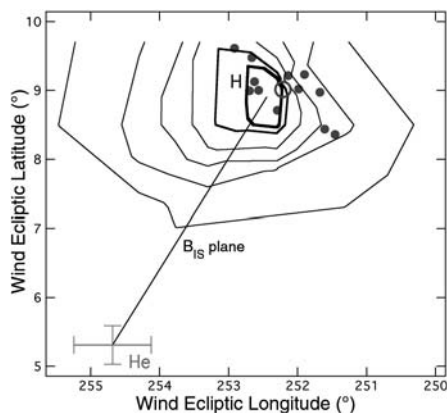
Fig. 2. H flow direction determination. Directions with χ^2 = 1.14 (bold line), 1.16, 1.21, 1.5, and 2.0 from the maximum-absorption location method are shown with solid lines. Dots indicate the series of corrected directions derived from the line profile reconstruction method. The He flow direction and its error bars are shown for comparison. If the deflection is associated with a magnetically distorted heliosphere, the H and He flow directions define the interstellar magnetic field plane.

Fig. 3. A schematic view of the heliosphere in the case of a B_{IS} inclined with respect to the flow direction [adapted from (24) and (25)]. Neutral (red arrows) and plasma (electrons and ions, black arrows) flows are sketched in the plane containing B_{IS} (dashed lines) and the wind flow vector. The secondary flow of H atoms (marked 2) is generated between the bow shock and the heliopause in a region between the Sun-wind axis and the displaced stagnation line (green dashed line). According to such a scheme, the plane containing the primary flow (nondeviated, marked 1) and the secondary flow also contains the magnetic field, and the secondary flow arrival direction lies between the wind axis and the field direction.
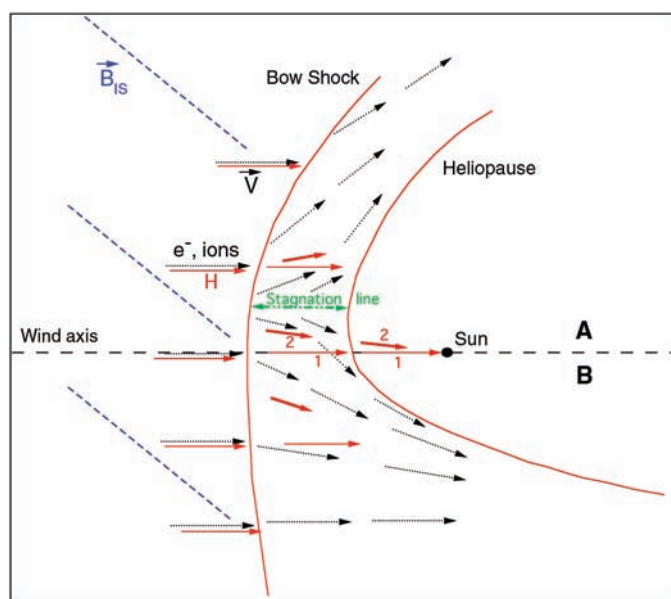
axisymmetric case (no magnetic field or parallel or perpendicular magnetic field) and the general case ($0° \ll \alpha \ll 90°$) is that the stagnation line (which separates the ions deflected on both sides of the heliopause) is no longer aligned with the Sun-wind axis but is offset. As a consequence, a larger number of secondary atoms able to reach the Sun (with the ion velocity vector directed toward the Sun before charge transfer) are formed on one side of the Sun-wind axis and form a deflected flow. The gas that is observed in the inner heliosphere is the sum of population 1 (nondeviated) and population 2 (deviated), and thus is itself deviated, although to a lesser extent, which depends on the relative contributions of the two fluxes. The departure of this average flow from the He flow is an imprint of the charge-exchange processes in the nonaxisymmetric outer heliosphere.

Three constraints on the direction of B_{IS} can be derived. First, B_{IS} is contained in the plane defined by the H and He flow vectors; that is, B_{IS} is perpendicular to $(\lambda, \beta) = (167°, -30°)$. Second, according to models, draping of magnetic field lines around the asymmetric heliopause is such that the high-pressure side of the heliosheath is opposite to the displaced stagnation line (Fig. 3). The other side, which contains the stagnation line, is filled with a less compressed flow of plasma and secondary neutrals and is the low-pressure region. The magnetic field from the interstellar side toward the inner heliosphere is thus oriented like the secondary flow of neutral H with respect to the wind axis but further away. The third constraint comes from the conditions on the angle α between B_{IS} and the bulk velocity V. Assuming that α is between 30° and 60°, an estimate range for the ecliptic coordinates of B_{IS} is $\lambda = 30°$ to 60°, $\beta = -30°$ to $-60°$ (or the opposite

direction). In galactic coordinates, this translates to (l, b) = (205° to 240°, $-38°$ to $-60°$), which can be compared with the spatial distribution of the local interstellar cloudlets derived from interstellar absorption lines recorded in the spectra of nearby stars (25, 26). The projection of B_{IS} onto the galactic plane is more or less tangent to the boundary of the local interstellar cloud, in the region that is facing the neighboring cooler and faster G cloud (so-called because it is located on the galactic center side), as would be the case if the magnetic field lines were compressed between the two cloudlets (Fig. 4).

The most compressed part of the heliosheath on the upwind side is opposite to the direction of deflection and thus is toward lower ecliptic latitudes (less than 5°) and higher longitudes (more than 254°) as compared with the wind axis. This should influence the direction of energetic neutral atoms originating from charge transfer with the subsonic solar wind and with accelerated particles. On the other hand, an additional magnetic compression is expected to increase the density of secondary neutral species piling up at the interface, reinforcing the so-called hydrogen wall (8), and possibly explaining ultraviolet spectrometer Ly-α data recorded over the past 10 years, which suggest an H wall–related emission increase stronger than what self-consistent models without a magnetic field predict (27).

If the heliosphere is distorted as in Fig. 3 under the action of a magnetic field, then the heliosphere is more elongated toward increasing ecliptic latitude. Voyager 1, which is at about 90 AU and is heading toward the northern ecliptic hemisphere, would be moving toward an elongated part of the termination shock. Indeed, such a configuration has been invoked recently

(28, 29) to reconcile all kinds of data recently collected (30–32) and to explain how Voyager 1 can detect energetic particles accelerated at the shock barrier without having crossed it yet.

References and Notes

1. R. Lallement, P. Bertin, *Astron. Astrophys.* **266**, 479 (1992).
2. P. Bertin, R. Lallement, R. Ferlet, A. Vidal-Madjar, *J. Geophys. Res.* **98**, 15193 (1993).
3. R. Lallement, R. Ferlet, *Astron. Astrophys.* **324**, 1105 (1997).
4. G. P. Zank, *Space Sci. Rev.* **89**, 413 (1999).
5. J. L. Bertaux, J. E. Blamont, *Astron. Astrophys.* **11**, 200 (1971).
6. M. K. Wallis, *Nature* **254**, 202 (1975).
7. T. E. Holzer, *Rev. Geophys. Space Phys.* **15**, 467 (1977).
8. V. B. Baranov, Y. Malama, *J. Geophys. Res.* **98**, 157 (1993).
9. R. Lallement, J. L. Bertaux, J. T. Clarke, *Science* **260**, 1095 (1993).
10. R. Lallement *et al.*, *Solar Wind 9 Am. Inst. Phys. Conf. Proc.* **471**, 205 (1999).
11. J. Costa *et al.*, *Astron. Astrophys.* **349**, 660 (1999).
12. E. Quémerais *et al.*, *J. Geophys. Res.* **104**, 12585 (1999).
13. V. V. Izmodenov *et al.*, *J. Geophys. Res.* **104**, 4731 (1999).
14. J. L. Bertaux *et al.*, *Sol. Phys.* **162**, 403 (1995).
15. E. Quémerais, V. Izmodenov, *Astron. Astrophys.* **396**, 269 (2002).
16. T. E. Woods, W. Kent Tobiska, G. J. Rottman, J. R. Worden, *J. Geophys. Res.* **105**, 27195 (2000).
17. P. Lemaire *et al.*, in *Proceedings of the SOHO 11th Workshop* (European Space Agency Special Publication 508, European Space Agency Publications Division, Noordwijk, Netherlands, 2002), p. 219.
18. M. Witte, *Astron. Astrophys.* **426**, 835 (2004).
19. J. Vallerga *et al.*, *Astron. Astrophys.* **426**, 855 (2004).
20. G. Gloeckler *et al.*, *Astron. Astrophys.* **426**, 845 (2004).
21. R. L. McNutt, J. Lyon, C. C. Goodrich, M. Wiltberger, *Solar Wind 9 Am. Inst. Phys. Conf. Proc.* **471**, 823 (1999).
22. T. J. Linde, T. I. Gombosi, P. L. Roe, K. G. Powell, D. L. DeZeeuw, *J. Geophys. Res.* **103**, 1889 (1998).
23. R. Ratkiewicz, A. Barnes, H.-R. Müller, G. P. Zank, G. M. Webb, *Adv. Space Res.* **29**, 433 (2002).
24. N. Pogorelov, G. P. Zank, T. Ogino, *Astrophys. J.* **614**, 1007 (2004).
25. R. Lallement, R. Ferlet, A. M. Lagrange, M. Lemoine, A. Vidal-Madjar, *Astron. Astrophys.* **304**, 461 (1995).
26. S. Redfield, J. L. Linsky, *Astrophys. J.* **534**, 825 (2000).
27. E. Quémerais, J.-L. Bertaux, R. Lallement, B. R. Sandel, V. Izmodenov, *J. Geophys. Res.* **108**, 8029 (2003).
28. J. R. Jokipii, J. Giacalone, J. Kóta, *Astrophys. J.* **611**, L141 (2004).
29. E. C. Stone, COSPAR, *Adv. Space Res.*, in press.
30. S. M. Krimigis *et al.*, *Nature* **426**, 45 (2003).
31. F. B. McDonald *et al.*, *Nature* **426**, 48 (2003).
32. L. F. Burlaga, N. F. Ness, F. B. McDonald, J. D. Richardson, C. Wang, *Astrophys. J.* **582**, 540 (2003).
33. The SOHO mission is a European Space Agency–NASA international cooperation. SWAN was financed in France by the Centre National d'Etudes Spatiales with support from the French National Center for Scientific Research (CNRS) and in Finland by Tekes and the Finnish Meteorological Institute. The data were obtained thanks to the help of the Experiment Operation and Flight Operation Teams at the Goddard Space Flight Center.

Fig. 4. Interstellar cloudlets around the Sun in the galactic plane [sketch adapted from (26) and (27)]. The galactic center direction [galactic longitude ($l_{ii} = 0°$)] and the anticenter ($l_{ii} = 180°$) are indicated. The local interstellar cloud (LIC) is surrounded by masses of gas with different velocities, temperatures, and abundances. Dot-dashed lines are the projections onto the galactic plane of the inferred B_{IS} in the two cases $\alpha = 30°$ and $\alpha = 60°$, which are considered as limits. αCen, alpha Centauri; 36 Oph, 36 Ophiuchi.